EVALUATION OF A COMPRESSION-LOADED-STITCHED-MULTI-BAY FUSELAGE PANEL WITH BARELY VISIBLE IMPACT DAMAGE*

Donald J. Baker
Vehicle Technology Directorate - ARL
NASA Langley Research Center
Hampton, Virginia 23681

Jian Li
Structural Integrity Department
The Boeing Company
Mesa, Arizona 85215

ABSTRACT

The experimental results from a stitched VaRTM carbon-epoxy composite panel tested under uni-axial compression loading are presented along with nonlinear finite element analysis prediction of the response. The curved panel is divided by frames and stringers into six bays with a column of three bays along the compressive loading direction. The frames are supported at the frame ends to resist out-of-plane translation. Back-to-back strain gages are used to record the strain and displacement transducers were used to record the out-of-plane displacements. In addition a full-field-displacement measurement technique that utilizes a camera-based-stereo-vision system was used to record the displacements. The panel was loaded to 1.5 times the predicted initial buckling load (1^{st} bay buckling load, P_{cr}) from the nonlinear finite element analysis and then was removed from the test machine for impact testing. After impacting with 20 ft-lbs of energy using a spherical impactor to produce barely visible damage the panel was loaded in compression until failure. The buckling load of the first bay to buckle was 97% of the buckling load before impact. The stitching constrained the impact damage from growing during the loading to failure. Impact damage had very little overall effect on panel stiffness. Panel stiffness measured by the full-field-displacement technique indicated a 13% loss in stiffness after impact. The panel failed at 1.64 times the first panel buckling load. The barely visible impact damage did not grow noticeably as the panel failed by global instability due to stringer-web terminations at the frame locations. The predictions from the nonlinear analysis of the finite element modeling of the entire specimen were very effective in the capture of the initial buckling and global behavior of the panel. In addition, the prediction highlighted the weakness of the panel under compression due to stringer web terminations. Both the test results and the nonlinear predictions serve to reinforce the severe penalty in structural integrity caused by the low cost manufacturing technique to terminate the stringer webs, and demonstrates the importance of this type of sub-component testing and high fidelity failure analysis in the design of a composite fuselage.

* Presented at the American Helicopter Society 61^{st} Annual Forum, Grapevine, TX, June 1-3, 2005.
This research was partially funded by the Aviation Applied Technology Directorate under Technology Investment Agreement No. DAAH10-02-2-00002. The U.S. Government is authorized to reproduce and distribute reprints for Government purposes not withstanding any copyright notation thereon."

Introduction

To improve the cost and weight savings of composite helicopter structures it will be necessary to reduce the conservatism that is used now in the design and analysis process. However, the cost and weight savings cannot be realized without a better understanding of the structural integrity issues associated with unitized composite structures. A high fidelity failure analysis methodology was previously proposed to analyze unitized composite structures [1, 2]. The objective of the proposed method in Reference 1 and 2 was to understand the global nonlinear behavior of the entire structure due to the interactions among its components and define local failure modes at the joining locations of the structural components. One stitched composite panel that was cut from a composite fuselage tool proof article has been loaded to 1.5 times the initial buckling load, P_{cr}, and the results have been compared in Reference 3 to the high fidelity analysis of Reference 1. Additional experimental results are shown in Reference 4. After the initial test, the panel was impacted to produce barely visible damage. The purpose of this paper is to determine the effect of the barely visible impact damage on the structural response of the panel. The strain results from the full-field displacement measurement and the strain gages results for before and after impact will be compared. The buckling sequence will be identified from the full field-field measurement technique

Test Panel

The stitched composite panel, to be identified as *C-1* in the rest of this paper, contains three stringers and two frames as shown in Figure 1. The test panel was cut from a fuselage tool proof article that was manufactured from stitched, warp knit and plain weave AS4 carbon fiber performs infused with SI-ZG-5A resin system using the Vacuum assisted Resin Transfer Molding (VaRTM) process. The skin laminates are a $[\pm 45^{wk}/0^{pw}]_s$ or $[\pm 45^{wk}/0^{pw}0^{pw}]_\$$ for the 0.040-in. and 0.056-in. thick laminates respectively. The subscripts "s" and "$" denote mid-plane and mid-ply symmetry for the plies in the [ ], respectively. The $\pm 45^{wk}$ represents two warp knit plies with the fibers in the ±45° directions with each ply thickness of 0.006-in. The 0^{pw} represents a single plain weave ply and is considered as [0/90] with the nominal ply thickness of 0.004-in for each ply. The stringers are a $[\pm 45^{wk}/0^{pw}]_s$ laminate while the frame is a $[0^{pw}/45^{pw}/0^{pw}]_s$ laminate. The skin is stitched together and the frame and stringer flanges are stitched to the skin. The stringer leg and the web of the frames are also stitched. The panel is 15.57-inches wide with a 55.9-inch radius in the width direction. The stringer vertical web terminates before the frame flange at each frame while the stringer flanges continue under the frame flange. For testing the panel ends were potted with 1-inch thick filled epoxy and were machined flat and parallel to the 28.4-inch dimension shown in Figure 1a. A 1-inch long section of the frame flange located at FS 145 and 154 was removed from each end and a 1-inch square, .062-inch thick, aluminum plate was bonded to each side of the web for reinforcement for a link to attach to the frame to resist the out-of-plane displacement at the frame ends.

Instrumentation

Three measurement techniques were utilized to determine the response of this panel:

Strain gages – Common off the shelf axial and rosette strain gages were used on the panel. Panel *C-1* contains 12 back-to-back rosettes located in the center of each bay and six back-to-back axial gages across the center of the panel located on the skin side and flange of the stringers. Gage numbers 1 through 21 are located on the stringer/frame side or inside-mold-line (IML) side and gages 22 through 42 are located on the skin or outside-mold-line (OML) side.

Displacement transducers – Linear variable displacement transducers (LVDT) were utilized to measure the displacements at selected locations. A LVDT was used at the center of each of the lower four bays to measure the out-of-plane displacements. A single LVDT was placed at the intersections of the centerline stringer and each frame. Two LVDT's were used to measure the panel end shortening.

Three-dimensional Video Image Correlation System (VIC-3D) - This system is a full-field-displacement measurement technique [5] that utilizes a camera-based stereo-vision system. VIC-3D[2] is a non-intrusive system that uses a contrasting speckle pattern (e.g., black and white paint) applied to the specimen to provide dense features that can accurately be tracked between different cameras and during deformation. Images of the changing pattern on the test specimen surface are recorded on a computer with the stereo-vision system at user specified time intervals. It is also possible to take data in a local area, e.g., in the vicinity of a notch or impact site, with a second camera based system while taking data on a global area. This will give higher resolution to the displacements in the local area of interest.

The skin surface of Panel *C-1* was painted white and a black spackle pattern was applied to the panel. A spackle pattern with a higher density was applied to the area around the impact site.

[2]VIC-3D system supplied by Correlated Solutions, Inc., W. Columbia, SC

To determine the geometry (profile) of the test specimen just prior to testing, an image of the unloaded specimen is taken as the reference. The specimen shape is determined by the analysis software from the image, and a best fit plane is fit to the image data using 8,000 to 10,000 data points. The best-fit plane is then used as the x-y plane of a new coordinate system, and the specimen shape data can be plotted as a three-dimensional color-coded contour plot, which permits visual identification of defects.

The VIC-3D analysis software converts the image data taken during a test to the full field u, v, and w displacements. Since the displacements are known, the strains can also be computed. The results can be displayed as displacement or strain contours in 2D or 3-D projections on the deformed or reference surface. Two-dimensional contour plots can also be developed. Options exist that allow extraction of displacement and/or strain results at a point in the image or along a line on the image. Selecting a line on the surface will give the profile of the panel cross-section or all displacements and strains at a pre-selected load. The line location is approximated by selecting two points on the screen. At the present it is not possible to select this line location or any point in direct relation to the specimen reference frame. Selecting a point on the screen is the only method.

For test specimens that have a curvature in a single direction, the software has an option for conversion to a cylindrical coordinate system.

Test Setup

Panel *C-1* is shown in Figure 2, in the test machine after completing the test to 1.5 times the predicted buckling load. The frame to react the out-of-plane loads is also shown in the figure. This frame is attached to the test machine lower platen and reacts the panel frame out-of-plane loads but not the frame rotations. The linkage shown from the panel allows the test specimen frames to rotate but not translate. The free edges of the panel were supported by knife edges as shown in the Figure 2.

The spackle pattern used for the VIC-3D system can be seen in Figure 2. The skin surface of the test specimen was painted white then a black paint spackle pattern was applied. Note the different spackle densities can be seen between the local and global areas, where the local area has smaller speckles and a higher density of speckles. The local area location was selected to encompass the impact site.

Test Results and Discussion

A profile of the panel was performed, using VIC-3D software, before it was removed from the test machine, to determine if the test to $1.5P_{cr}$ resulted in any permanent set. The panel profile matched the profile taken prior to the $1.5P_{cr}$ load test.

Impact

Panel *C-1* was placed under the impact tower shown in Figure 3 and a 5-lb weight with a 0.5-inch spherical radius impactor was dropped on the specimen. Lead shot bags was placed on and around the specimen to dampen the vibrations. The impact location was at the end of a center stringer termination adjacent to FS 154 on the Outer Mold Line (OML) side of the panel. The energy required to produce barely visible damage was determined on a different panel of the same design. The impactor was dropped 4-feet to give an energy level of 20 ft-lbs. Barely visible impact damage occurred on the specimen skin surface with the 20 ft-lbs of impact energy. A photograph of the impact site with the actual impact location is shown in Figure 4. The final impact site was 1/8-inch from the centerline of the panel. The profile of the contact force as determined from a load cell in series with the impactor is shown in Figure 5 and indicates a loss of stiffness as given by the contact force drop of approximately 150 lbs. after reaching the peak force of 908 lbs. The contact force recovered some but never exceeded the peak value of 908 lbs.

After impact and before any loading the profile of the impacted panel *C-1* was determined. The profile of the full panel did not show any significant changes due to the impact but results of the local area (3-inch by 4-inch) shown in Figure 6 indicates an impact dent depth of 0.008 to 0.010-inches deep. Deviations from the constant cross-section radius of 55.9-inches are shown in Figure 7 at a section through the impact site and at 2.0-inches from the impact site. This data indicates the dent is approximately 0.01-in. below the surrounding surface. This figure also indicated the cross-section radius is within 0.03-in. of the 55.9-in. radius.

Test to Failure

Displacements Panel *C-1* was loaded to failure at a low load rate of approximately 1,000 lbs. per minute. An obvious advantage of using the VIC-3D system is the full field recording of events at timed intervals through out the test. During loading, panel *C-1* had five of the bays that bowed out-of-plane in the positive direction (0.0 to over 0.01-inches) as shown in Figure 8a for $N_y = 0.75P_{cr}$ The upper R/H bay had out-of-plane displacements ranging from -0.01-inch to +0.01-inches as shown in the figure. The dashed lines superposed on the figures are the approximate locations of the frames and stringers. The positive displacement direction is away from the OML, or toward the viewer when looking at Figure 8a. Review of the image data for the

test to limit load indicated similar type of deformation patterns, except those images did not indicate an area of negative deformation between the two upper bays as shown in Figure 8a. It is possible that there was some damage under the stringer flange as the impact area was between the lower end of the stringer and the flange of the frame. Increasing the load to $N_y = 0.96P_{cr}$ the same five bays still bowed in the positive direction while the upper R/H bay changed into three half-waves as shown in Figure 8b. Increasing the load to $N_y = 1.006P_{cr}$ the upper R/H panel buckles as shown in Figure 8c. The only significant change in the other bays is the increase in size of the area of the positive out-of-plane displacement to over 0.02-inches. A second bay (middle L/H) buckled when the load was $N_y = 1.075P_{cr}$ as shown in Figure 8d. The second buckle was not present at the load of $N_y = 1.006P_{cr}$ although the presence of two positive displacement areas is noted. These areas could be the start of three half waves as seen in the upper R/H bay. The upper L/H and middle R/H bays increased in positive displacement as the load increases. The effect of loading was insignificant on the out-of-plane displacements of the lower two bays. This result was due to the fact that the lower skin was 40% thicker than the upper and middle bays (see Figure 1) and the outer two stringers on the lower two bays are twice the thickness of the other stringers. Increasing the load to 1.5 times the buckling load produces a deformation pattern as shown in Figure 8e. It appears that the deformation from the buckle in the upper R/H bay extends into the edge of the stringer. Increasing the load to $N_y = 1.63P_{cr}$ produced the deformation pattern shown in Figure 8f. This is the last image before maximum load of $N_y = 1.64P_{cr}$ is achieved. Note the major change between Figures 8e and 8f is in the upper L/H bay and the change in shape of the buckle in the upper R/H bay. The depth of the buckle in the upper R/H bays is increasing while the depth of the buckle in the middle L/H bay is decreasing. The change in shape of the deformations on the upper bays would indicate the center stiffener in the upper bay has lost some of its effectiveness. The contours of positive out-of-plane displacement shown in Figure 8f indicates the entire cross section is bending.

The global images provided a view of how the panel deformed as the load was applied. The appearance of the upper R/H bay appearing to deform in three half waves before "snapping" into half wave buckle represented the initial buckling event within the bays of the panel. The load as the first bay buckles is defined as the critical buckling load, P_{cr}. A review of all local images did not indicate any delamination or damage growth around the impact site.

Strain This section of the paper will compare the strain gage or displacement results before and after impact with the results extracted from the VIC-3D images. Ideally the strain calculations from the VIC-3D images should be performed at locations where the surface is flat. For Panel *C-1* all strain calculations for the following figures are performed at the strain gage locations. The strain gages on the surface at the point of the strain calculation could introduce some error in the strain calculations from the VIC-3D image data.

The deformed shape of the panel at $N_y = 1.63P_{cr}$ (last image before failure) is shown in Figure 9a along with the strain gage locations where the results are given in Figures 9b through 9f. Strain results from gages 1 & 22 in the first bay to buckle are shown in Figure 9b. This figure and subsequent figures will include strain gage results from before impact, after impact, and strain results extracted from the VIC-3D images taken during the test to failure after impact. The critical buckling load, P_{cr}, used to normalize the data is the actual buckling load determined in the test. The critical buckling load for the post-impact test is approximately 97% of the buckling load for the before impact test. Results shown in Figure 9b indicate bending in the panel starts at approximately $N_y = 0.65P_{cr}$. The results for the gages from before and after impact are identical from initial loading to failure. The strain results extracted from VIC-3D, shown by the curve with a diamond symbol in Figure 9b, also match the strain, determined by strain gages to the buckling load. From the buckling load to failure the VIC-3D strain data deviates from the gage data by increasing at a higher rate than the strain gage results as load increases to failure. One possible explanation for this deviation is that as the buckle grows deeper the surface that is being photographed is approaching the limits of the depth of field for the particular camera/lens setup.

Strain results for the upper L/H bay are shown in Figure 9c. The strain gage results for gages 4 and 25 from before and after impact appear to be identical. The bay started to bend at approximately $N_y = 1.2P_{cr}$ and continued to bend until failure. The strain results identified by a line with a diamond symbol was extracted from VIC-3D images compares well the strain gage data up to failure.

Results at the point when the second bay buckles (middle L/H side) are shown in Figure 9d, for strain gages 10 and 31. The strain gage results from before impact test and after impact test match up to the failure point. The strain computed from the VIC-3D images compared well with the strain gage results up to the buckling point of the bay. The VIC-3D results indicated a step in the strain when the bay snapped into a single half wave of approximately twice the strain indicated from the strain gages and then maintained approximately the same slope as the strain gages.

The result for strain gages 20 and 41, which are back-to-back gages located on the centerline stringer flange (gage 20) and OML (gage 41) at the panel center, are shown in Figure 9e. The strain gage (41) on the skin side indicates a step in the strain when the middle L\H bays buckles. The slope of the load-strain curve changes when the bay buckles and indicates an increasing strain on the OML side. Post-buckling stiffness of the skin is lower than the pre-buckling skin stiffness. The load strain curve extracted from the VIC-3D images is shown as a solid line with a diamond symbol and follows the same trend as strain gage on the OML side.

The panel end shortening is shown in Figure 10. The dashed lines in Figure 10 are the results from LVDT data, while the solid line is for data extracted from the VIC-3D images. The end shortening per unit length for the LVDT data is determined by dividing the overall change in the distance between the platens by the panel unloaded length (28.4-inches). With the VIC-3D data the displacement and point location at two points is determined and the change in length is divided by the distance between the points.

A least squares fit has been calculated for each set of data from P/P_{cr} = 0.1 to 0.9. There is a 2% difference between the slopes of the before impact and after impact curves as determined by LVDT's. As indicated in Figure 10, panel stiffness is higher as determined by the VIC-3D data than the stiffness determined from the LVDT data. The slope of the before impact VIC-3D curve is 135% of the slope of the curve for before impact with LVDT's. The slope of the VIC-3D curve for after impact is 87% of the slope for the before impact.

Final Failure

Panel *C-1* failed at $N_y = 1.64P_{cr}$ and a photograph of the failed specimen in the test machine is shown in Figure 11. The panel failed by folding in the skin adjacent to the flange of frame at FS 154. The edge view detail shows the out-of-plane displacement. The impact site is in the failure line but did not appear to have any significant effect on the failure mode. Close up photographs of the area at the impact site indicate cracks/crazing radiating from the impact site.

Analysis Comparison

Extensive comparisons between nonlinear analysis and test results were presented in Reference 3 through the buckling of the first two bays. Good predictions for initial buckling, deformation and strains were obtained from the nonlinear analysis.

From the actual measurement and location of the impact damage shown in Figure 4, an accurate representation of the impact damage was created through local modeling that takes into account the damage size and location with respective the center stringer centerline and distance from FS 154. A close-up of the finite element model of the impact site is shown in Figure 12. The nonlinear analysis used in reference 3 was modified to include the barely visible damage and was used to predict the panel response. Tie boundary condition was used to enforce displacement compatibility between the local model and the global model developed in Reference 3. The axial strain (y-direction) distribution at the OML ply predicted by the nonlinear analysis at $P=1.63P_{cr}$.is shown in Figure 13. The results in Figure 13 demonstrate a global instability along FS 154 due to stringer web terminations. Also of interest is the fact that at the stringer termination location, the compression strain has a higher compression strain than anywhere else including the impact damage location. The predicted deformed shape of folding along FS 154 shown in Figure 13 compares well with the experimental observation shown in Figure 11.

Concluding remarks

A stitched VaRTM multi-frame multi-stringer panel has been tested and analyzed in uni-axial compression. Panel buckling response while under compression load was recorded with strain gages, displacement transducers and 3D Vision Correlation System (VIC-3D. This test series show that there was good correlation between the three methods used to investigate panel buckling under load. The VIC-3D method showed several advantages over contemporary strain gauges and displacement transducers such as noninvasive to structure, equipment is not damaged when failure occurs, and preparation time is significantly reduced. One of the main features that VIC-3D has over other methods is to detect buckling during loading phase while recording at the global level and not at local or micro level. This means that the high strain locations need to be known on the panel before attaching strain gauges or displacement transducers is eliminated. Even the preciseness of locating strain gauges or displacement transducer within tight tolerances can be eliminated by using VIC-3D.

This work also shows that stitched composite panels have a high resistance to grow damage when after impacted on a stringer to skin interface. This was verified by the panel failure mode which was away from the damage site. In addition to the above techniques used to determine impact damage effect to stiffened panels, high fidelity failure analysis should be the norm for designing light weight highly efficient structures.

Acknowledgements

This effort was conducted as part of the Survivable Affordable Repairable Airframe Program conducted under the auspices of the U.S. Army Aviation Applied Technology Directorate (AATD) at Fort Eustis, VA, and the Rotorcraft Industry Technical Association (RITA) under contract number DAAH10-02-2-0002. The views and conclusions contained in this document are those of the authors and should not be interpreted as representing the official policies, either expressed or implied, of the Aviation Applied Technology Directorate or the U.S. Government. We would like to thank Mr. Stephen L. Guymon of Boeing for his review and valuable comments absorbed into the paper.

References

1. Li, J., Dávila, C. G. And Chen, T. "High Fidelity Failure Analysis for A Composite Fuselage Section," Proceedings of the American Helicopter Society 57th Annual Forum, Washington, DC, May 9-11, 2001.

2. Li, J. "High Fidelity Structural Integrity Analysis Methodology for Composite Rotorcraft Structures," Proceedings of the 48th International SAMPE Symposium and Exhibition, Long Beach, California, May 11-15, 2003, pp. 1430-1440.

3. Li, J and Baker, Donald J., "Test and Analysis of a Composite Multi-Bay Fuselage Panel under Uni-axial Compression," Proceedings of the 45th AIAA/ASME/AHS/ASC Structures, Structural Dynamics and Materials Conference, AIAA-2004-2056, Palm Springs, CA, April 19-24, 2004.

4. Baker, Donald J., "Experimental Results From Stitched Composite Multi-Bay Fuselage Panels Tested Under Uni-Axial Compression," NASA TM/TM-2004-213262, U.S Army ARL-TR-3233, September 2004.

5. Helm, J. D., McNeil, S. R., Sutton, M. A., "Improved Three-Dimensional Image Correlation for Surface Displacement Measurement," Optical Engineering, Vol. 35, No 7, July 1996, pp1911-1920.

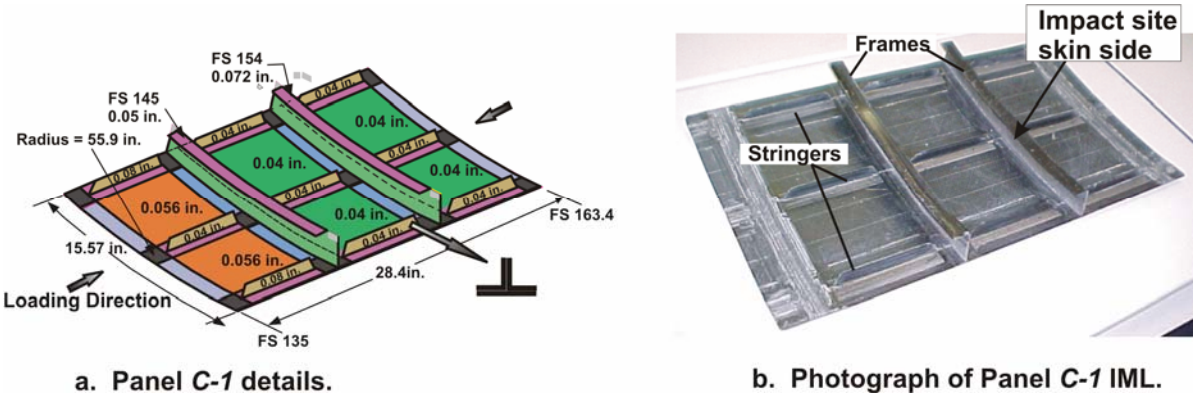

.

Figure 1 – Panel *C-1* details.

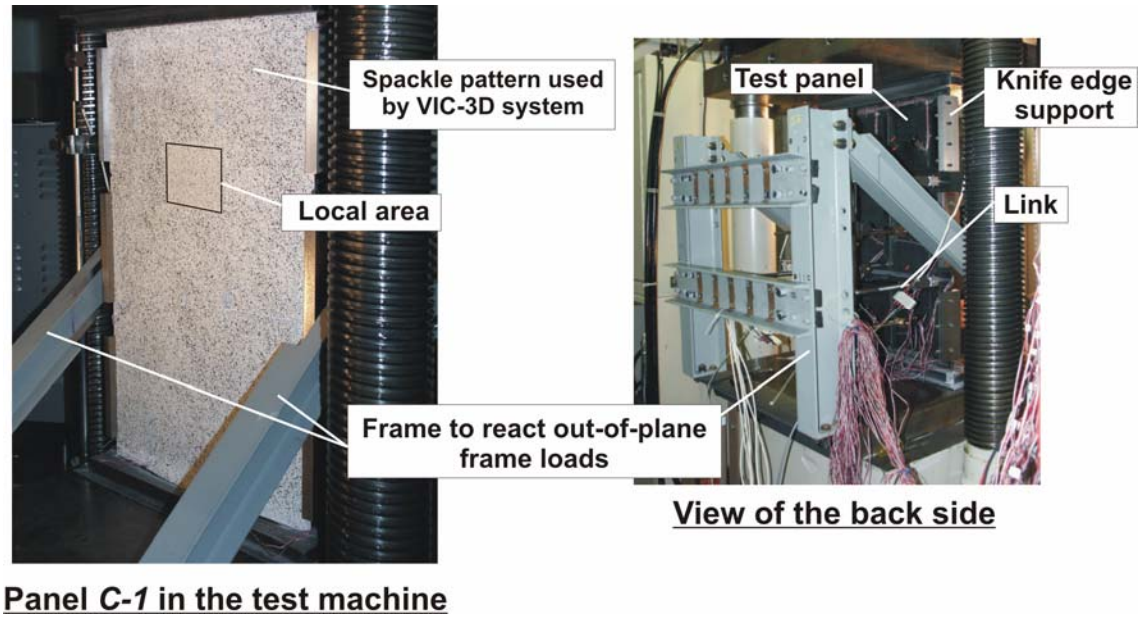

Figure 2 – Photographs of panel C-1 in test machine.

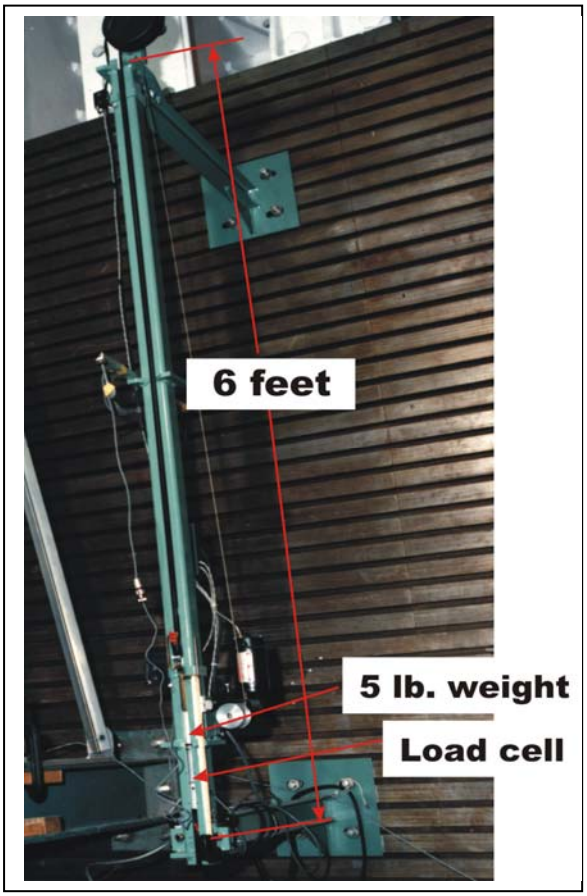

Figure 3 – Drop tower.

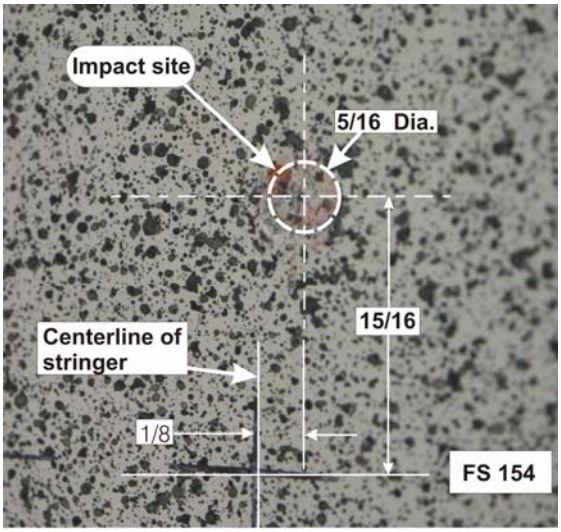

Figure 4 – Location of impact damage.
(Dimensions in inches)

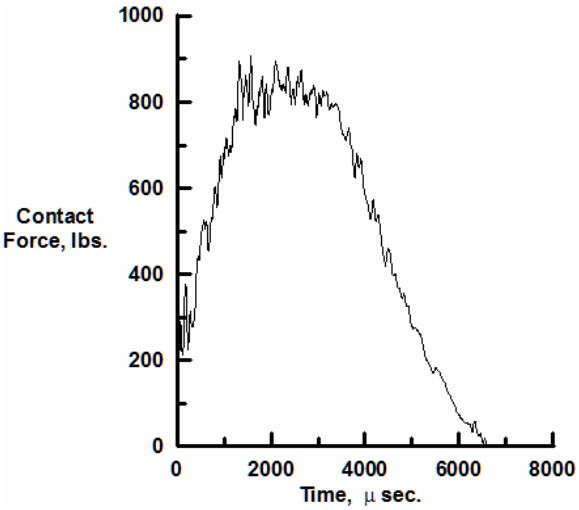

Figure 5 - Impactor contact force as function of time.

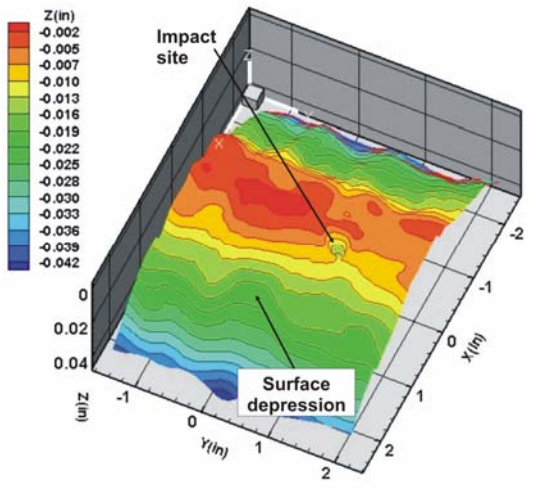

Figure 6 – Surface geometry after impact.

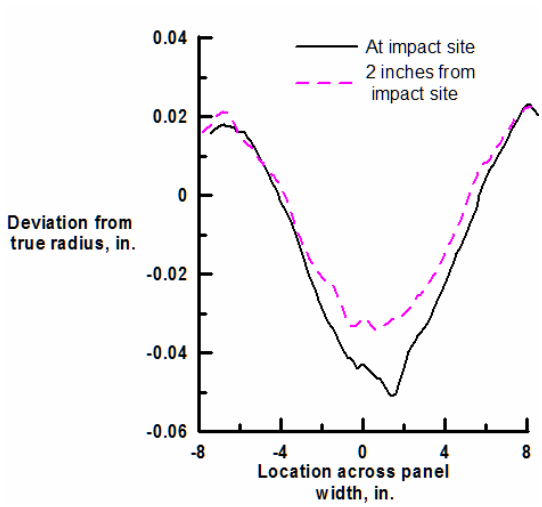

Figure 7 – Deviation from true radius across panel.

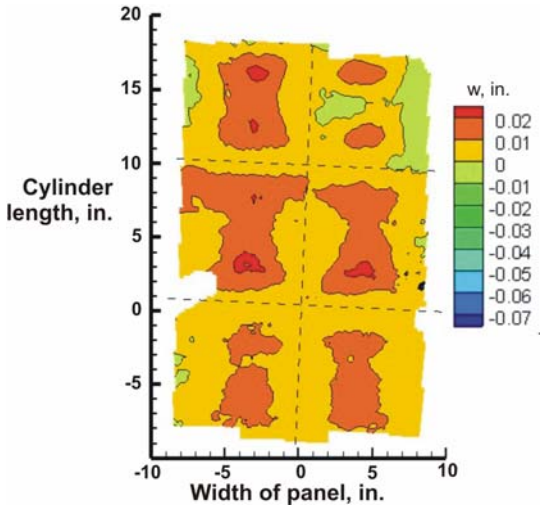

Figure 8b – Out-of-plane displacements for $N_y = 0.96P_{cr}$.

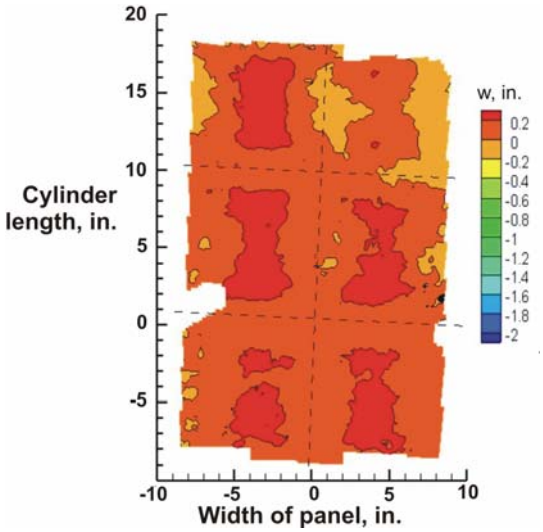

Figure 8a – Out-of-plane displacements for $N_y = 0.75P_{cr}$.

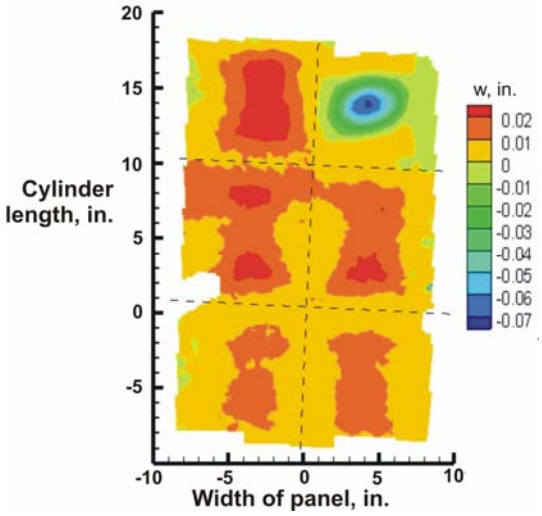

Figure 8c – Out-of-plane displacements for $N_y = 1.006P_{cr}$.

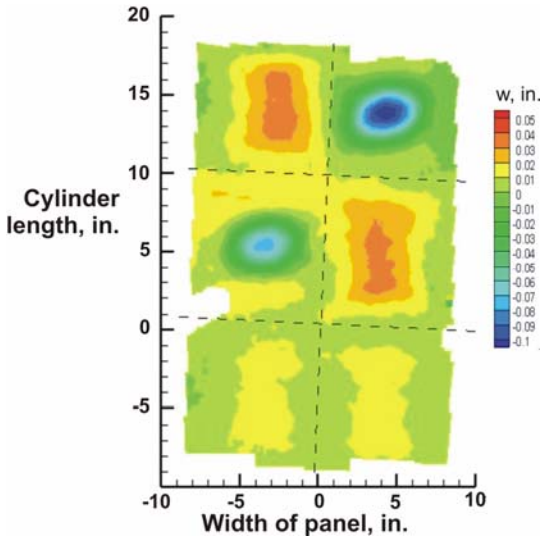

Figure 8d – Out-of-plane displacements for $N_y = 1.075P_{cr}$.

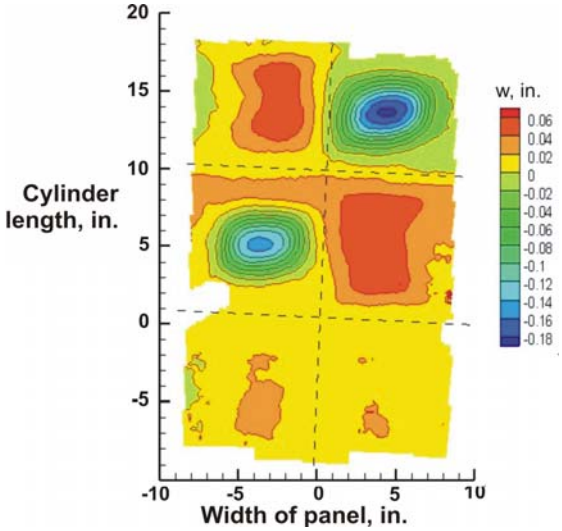

Figure 8e – Out-of-plane displacements for $N_y = 1.50P_{cr}$.

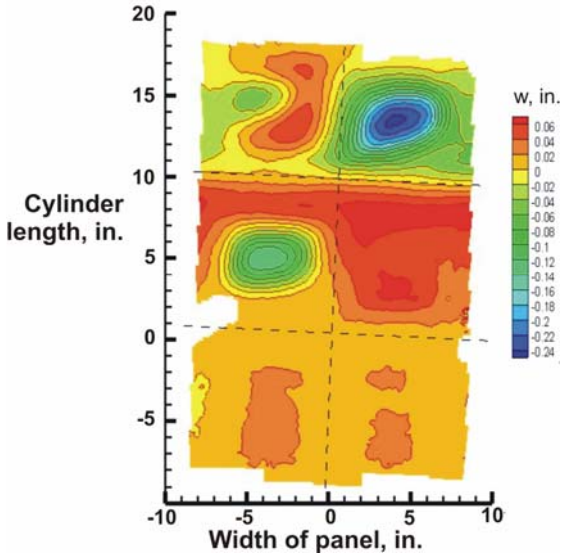

Figure 8f – Out-of-plane displacements for $N_y = 1.63P_{cr}$

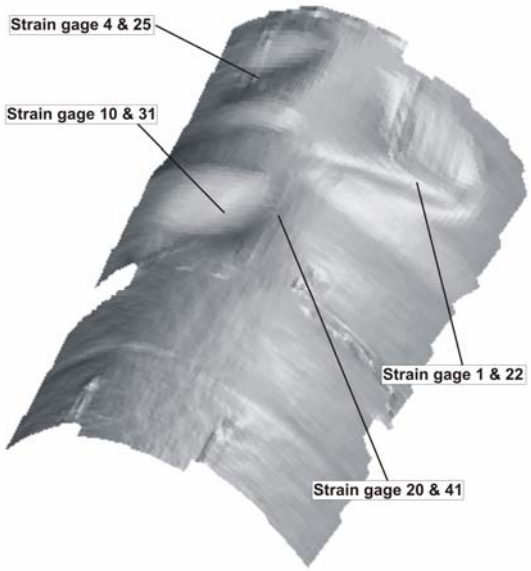

.

Figure 9a – Deformed shape of panel at $N_y = 1.63P_{cr}$.

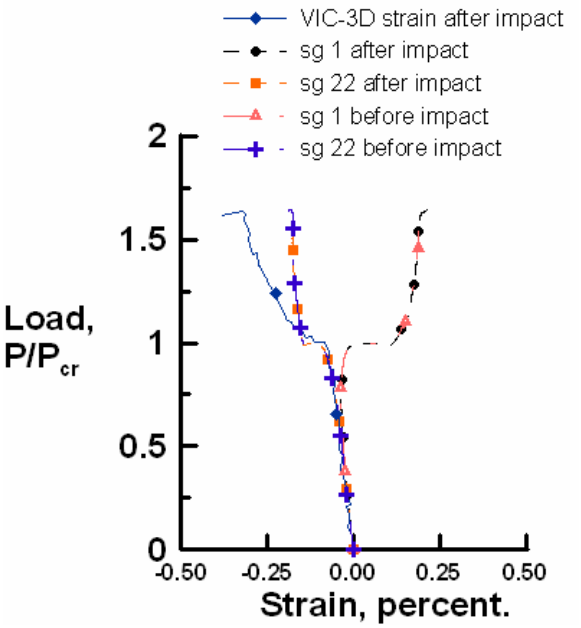

Figure 9b – Strain as a function load for strain gages 1 and 22.

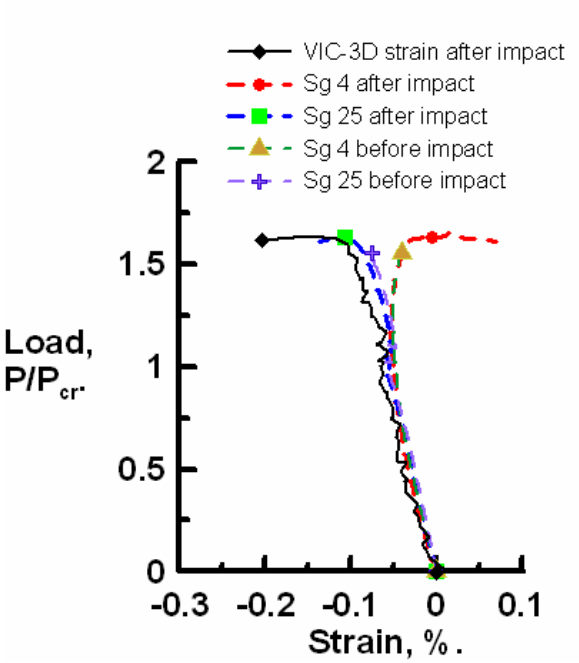

Figure 9c - Strain as a function load for strain gages 4 and 25.

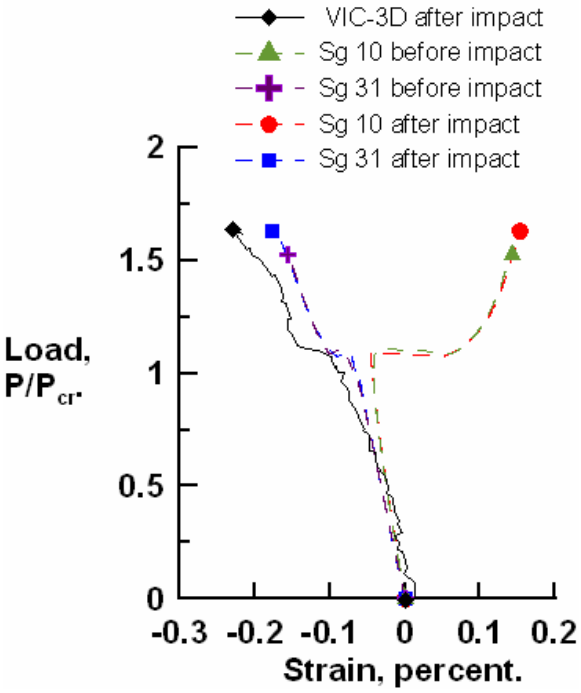

Figure 9d - Strain as a function load for strain gages 10 and 31.

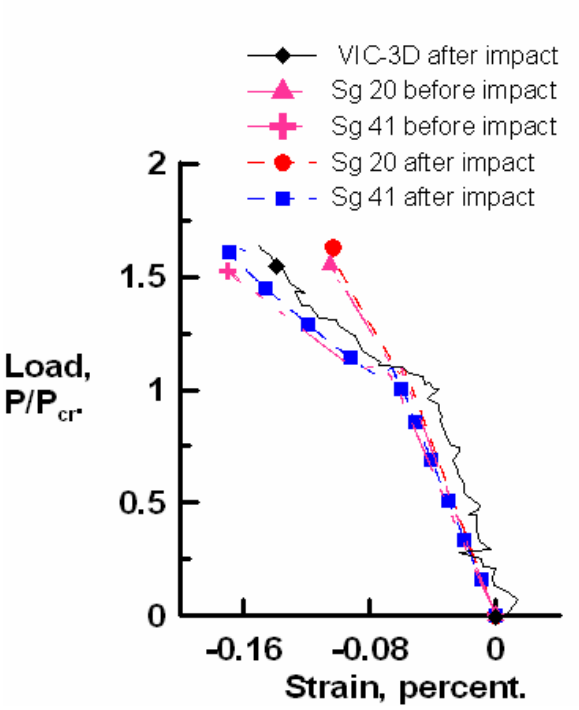

Figure 9e – Strain as a function of load for strain gages 20 and 41.

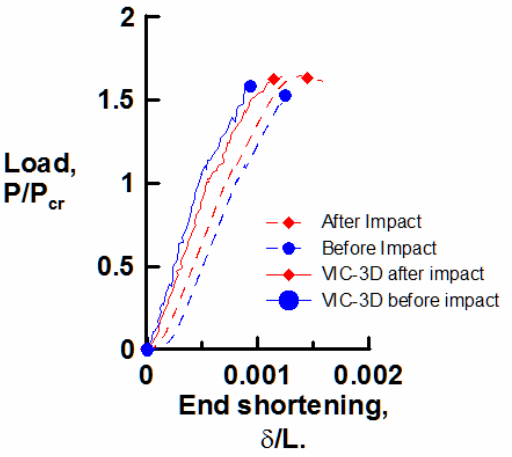

Figure 10 - Panel end shortening

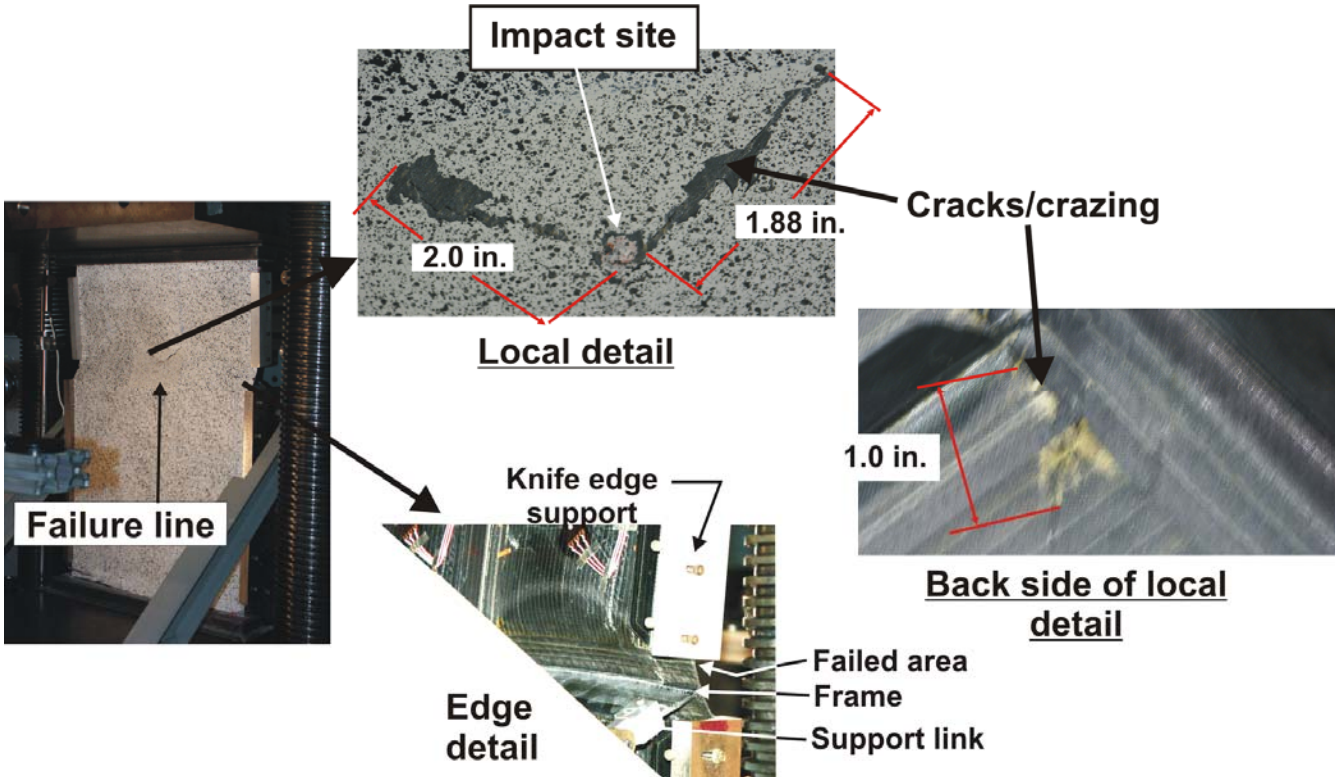

Figure 11 - Failed panel C-1.

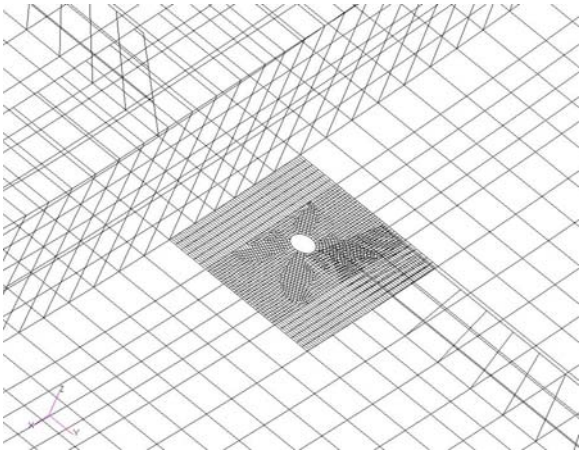

Figure 12. Barely visible impact damage modeling for panel *C-1*.

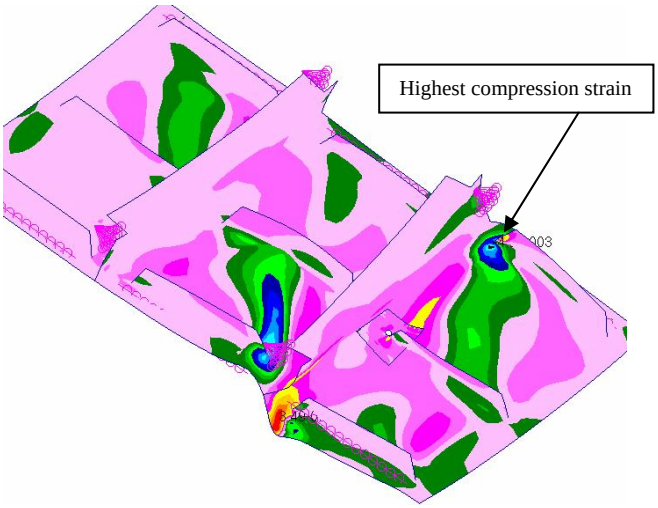

Figure 13. Axial strain prediction by nonlinear analysis at $N_y=1.63P_{cr}$.